Heliyon 9 (2023) e18092

Contents lists available at ScienceDirect

Heliyon

journal homepage: www.cell.com/heliyon

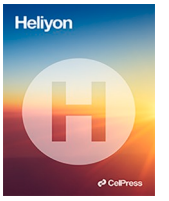

Energy simulation and CFD coupled analysis for the optimal operation of combined convection and radiant air conditioning considering dehumidification

Tatsuhiro Yamamoto *, Akihito Ozaki, Keigo Aratsu, Ryo Fukui

Faculty of Human-Environment Studies, Kyushu University, 744 Motooka Nishi-ku, Fukuoka City, Fukuoka, 819-0395, Japan

ARTICLE INFO

Keywords:
Energy simulation
Computational fluid dynamics
Air conditioner
Radiant panel
Dehumidification
Power consumption

ABSTRACT

The use of radiant panels in homes has increased recently because they do not cause a drafty feeling, unlike air conditioners. However, air conditioners are more power-efficient than radiant panels and have a higher coefficient of performance (COP). Therefore, combining radiant panels and air conditioning can provide an optimal solution for thermal control in residences. Energy simulation (ES) and computational fluid dynamics (CFD) can be used to simulate such environments. ES is suitable for non-steady state calculations, and combined with appropriate modeling, enables an accurate estimation of power consumption. Effective dehumidification becomes necessary, during summer as the relative humidity in a room increases. Both air conditioners and radiant panels can achieve this. This study developed a simulation tool that incorporates the effects of dehumidification. Based on a relative evaluation, a case was proposed where both energy efficiency and comfort were satisfied by jointly using air conditioners and radiant panels. The study found that a small number of panels could achieve the most balanced operation. The results of this study can serve as a reference for general housing, and the developed simulation tool can be applied to product development and building material design.

1. Introduction

The rapid advancement of science and technology has led to a gradual increase in energy demand in recent years. In line with sustainable development goals [1,2], numerous countries have undertaken active measures to reduce energy consumption [2], including the promotion and use of renewable energy sources. Economic globalization and the greater adoption of renewable energy are expected to help mitigate CO_2 emissions in Gulf Cooperation Council (GCC) economies [3,4]. However, prior research has shown that high economic growth often reduces the rate of adoption of renewable energy consumption in nondemocratic countries [5].

Radiant panels have emerged as a promising solution for meeting both energy conservation and comfort requirements. Owing to their low draft and high air conditioning capacity, radiant panels offer efficient and comfortable thermal control in various settings, such as alcoves in libraries, airports, and small rooms serving as specially enclosed spaces for low-cost lodging in large cities [6]. Notably, radiant panels used in offices, such as ceiling radiant cooling panels, have demonstrated their capacity to save energy [7].

Although the residential use of radiant panels has gained popularity in recent years, their efficiency is not consistent because of the use of water-cooled heat pumps. To the best of our knowledge, a generic tool that can predict the power consumption (also called

* Corresponding author.
E-mail address: ymt@kyudai.jp (T. Yamamoto).

https://doi.org/10.1016/j.heliyon.2023.e18092
Received 26 April 2023; Received in revised form 28 June 2023; Accepted 6 July 2023
Available online 11 July 2023

Nomenclature

α	Heat distribution ratio [−]
C_p	Specific heat of air [J/kg·K]
γ	Specific gravity [kg/m^3]
V_i	Volume of i-zone [m^3]
T_i^*	Temperature at zone i [K]
$T_{s,i}$	Reference temperature for zone i [K]
q_{losti}	Heat loss from the wall surface [W]
Q_T	Heat input by air conditioner [W]
Q_P	Convective heat transfer of radiant panel [W]
Q_{AC}	Sensible heat from air conditioners [W]
q_i	Amount of heat distributed to zone i [W]
a_c	Convective heat transfer coefficient of panel surface [W/m^{2}K]
A	Panel surface area [m^2]
α_{AC}	Heat diffusion coefficient of air conditioner [−]
α_P	Heat diffusion coefficient of radiant panel [−]
$T_{i,j}$	Temperature at target surface j [K]
$\overline{c\gamma}$	Apparent heat capacity of the room, including furniture [J/m^3·K]
$S_{i,j}$	Area of target surface j [m^2]
$h_{i,j}$	Convective heat transfer coefficient of target surface j [W/m^{2}K]
V_o	Amount of outside air introduced [m^3/s]
$c\gamma$	Volume specific heat [J/m^3·K]
q_{wall}	Wall heat flux [W/m^2]
ρ_f	Density of fluid [kg/m^3]
$C_{P,f}$	Specific heat of fluid [J/kg·K]
y_c	Normal distance from the wall [m]
u_τ	Velocity scale based on wall shear stress [m/s]
T^+	Dimensionless temperature [−]
y^+_{fluid}	Dimensionless distance to turbulent water [−]
h_{wall}	Convective heat transfer coefficient of the wall surface [W/m^2·K]
q_{wall}	Heat flux at the wall [W/m^2]
t_{wall}	Surface temperature at wall [K]
t_{fluid}	Fluid temperature [K]
$F_{l,j}$	Morphology coefficient of surface l looking at surface j [−]
ε_j	Longwave emissivity of surface j [−]
ELR_j	Net radiation emitted by surface j [W/m^2]
S_j	Area of surface j [m^2]
$\alpha_{r,jk}$	Radiative heat transfer coefficient from surface j to surface k [W/m^{2}K]
ALR_j	Absorption capacity of surface j [W/m^2]
LI_c	Longwave radiation components from lights and fixtures [−]
LH_f	Longwave radiation component from human body [−]
NLR_j	Net radiation from surface j [W/m^2]

energy consumption in this paper) of residential radiant panels is not yet available. Although equipment characteristic models [8] exist to predict the power consumption of air conditioners, equivalent tools for residential radiant panels are still lacking, despite the growing demand for radiant panels in residences. Given that air conditioners are energy-efficient, they are expected to be used in combination with radiant panels.

Energy simulation (ES) is widely used in the field of architecture. Computational fluid dynamics (CFD), a type of computer-aided engineering tool, is also widely used for analyzing houses and offices [9,10], for studying energy-efficient designs for heat pumps [11], as well as to perform blood flow analyses in medical fields [12] and aerodynamic analyses of aircraft [13]. ES is an excellent tool for performing transient calculations for building construction, making it suitable for power consumption estimation. It is possible to calculate the power consumption of heating, ventilation, and air conditioning (HVAC) systems for office spaces using equipment models such as the life cycle energy management (LCEM) model [14]. A previous study reported an example of calculating the power consumption of HVAC in a secondary school [15]. In contrast, CFD is suitable for solving spatial distributions. Many CFD studies have been reported for both residential and office spaces [16], including studies on radiant air conditioning [17]. However, these analyses are often limited to steady-state conditions owing to computational constraints.

Coupled ES-CFD analyses were systematized and summarized by Zhai et al. [18,19], and have since been further developed because

ES and CFD are complementary [20]. Large-space transient analysis methods that enable sophisticated coupled ES-CFD calculations have been developed [21]. However, while power consumption calculations for residential heat pumps are often simplified, a coupled ES-CFD analysis for calculating power consumption in offices is still needed [22]. Recently, Yamamoto et al. [23] calculated the power consumption of air conditioners and demonstrated their potential application to residential buildings. Because heat pumps operate on similar principles as air conditioners, a similar method can be used to calculate the power consumption of radiant panels.

Using both highly efficient air conditioners and radiant panels in residential buildings would be desirable in the future. Yamamoto et al. [24] developed another method to accurately predict the thermal environment when jointly using air conditioners and radiant panels. However, this analysis method did not incorporate equipment models when calculating the power consumption considering the dehumidification of the air in the space, which can affect the predicted mean vote (PMV). Moreover, the heat distribution method developed by Yamamoto et al. [24] for the combined use of air conditioners and radiant panels is limited to calculating only the thermal environment [20] and, therefore, does not support energy calculations. In this study, power consumption of air conditioners and radiant panels was calculated using the equipment characteristic model developed by the Central Research Institute of the Electric Power Industry [23]. Additionally, unlike the conventional method, this study considered the contribution rate of heat to each zone in a macroscopic manner. This major feature differentiates the proposed method from the contribution ratio of the previously proposed indoor climate (CRI) approach [25]. Furthermore, the proposed method incorporates power consumption prediction or dehumidification, which is another advantageous feature over the CRI approach. All values used in the case study analysis were calculated, whereas some of those used in the accuracy verification were measured. Dehumidification was incorporated into the coupled ES-CFD analysis of the equipment characteristic model introduced by Yamamoto et al. [23], and its performance was verified. They developed a tool to calculate the environmental humidity of a target space by incorporating the dehumidification provided by radiant panels and air conditioners. Yamamoto et al. [20] provides all necessary information (e.g., measured values and analytical models. Although the follow-up report is based on this previous study [20], its focus on comfort and energy efficiency can be considered novel. Moreover, to the best of our knowledge, no other studies have considered the dehumidification provided by radiant panels. Therefore, the novelty of this study lies in the consideration of the effect of dehumidification on energy conservation and comfort from a heat perspective.

The objective of this study was to develop a coupled algorithm that considers dehumidification and can be used to investigate various scenarios related to energy efficiency and comfort. Furthermore, this study aimed to identify the optimal operation method through case studies conducted using the proposed algorithm. The accuracy of a power consumption prediction program that considers dehumidification was investigated through a coupled ES-CFD analysis. After evaluating the accuracy of predicted results, case studies were conducted on the basis of relative evaluations to optimize an operation strategy that satisfies both comfort and energy efficiency. The primary objective of this study was to develop a coupled algorithm that can consider dehumidification and can be used to examine various scenarios related to energy efficiency and comfort. The purpose of these case studies was not to determine the best operation method, as they focused only on a small portion of the model. Moreover, estimating dehumidification was not the only objective. As regards the building model and the case study, they are meaningless unless their accuracy has been established in a previous study [20]. The algorithm's major advantage is its incorporation of the dehumidification provided by radiant panels, which can lead to more accurate and efficient energy management. Finally, the current study is novel in that it deals with the coupled analysis when air conditioning and radiant panels are used jointly. Previous studies have only considered air conditioning or radiant panels, rather than their combination.

2. Mathematical formulation

2.1. Calculation of the heat quantity diffusion coefficient

The heat distribution ratio, which is the ratio between the sum of the heat losses from the wall surfaces of each zone and the heat loss from the temperature increase in the space by the overall heat input [24], is expressed in equation (1) as follows:

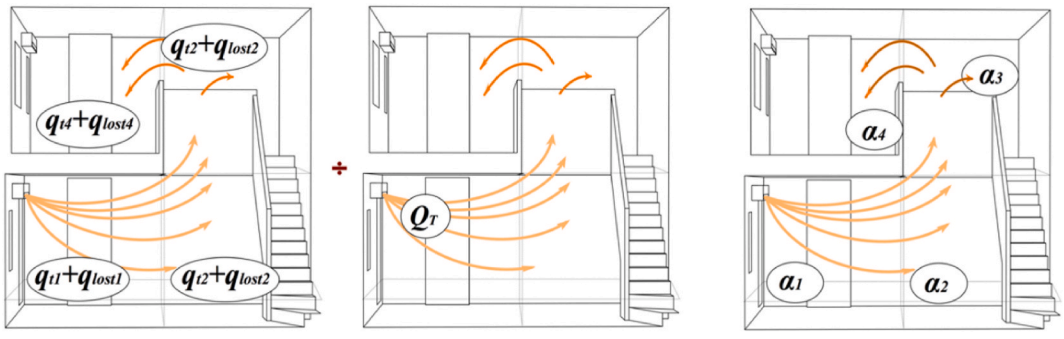

Fig. 1. Conceptual diagram of the heat distribution method [24].

$$i = \frac{C_p \gamma V_i \frac{\left(T_i^{'} - T_{s,i}\right)}{dt} + q_{losti}}{Q_T}. \tag{1}$$

The heat distribution ratio represents the contribution of each zone to the heat input and can be expressed in equation (2) as follows:

$$\sum_{i=1}^{n} \overline{\alpha}_i = 1. \tag{2}$$

Fig. 1 shows a conceptual diagram of the heat distribution method [24].
The heat input by the radiant panel is expressed in equation (3) as follows:

$$Q_P = a_c \bullet A \bullet (t_a - t_s). \tag{3}$$

The heat input, q_i, for each space is expressed in equation (4) as follows:

$$q_i = Q_{AC} \bullet \alpha_{AC,i} + Q_P \bullet \alpha_{P,i.} \tag{4}$$

The heat balance for the space is given by equation (5):

$$V_{oi} \overline{c\gamma} \frac{dT_i}{dt} = \sum_{j=1}^{J} S_{i\,,\,j} h_{i,j} \left(T_{i\,,\,j} - T_i\right) + V_o c\gamma (T_o - T_i) + q_{i.} \tag{5}$$

2.2. Calculation of the convective heat transfer coefficient

The convective heat transfer coefficient can be determined using equations (6) and (7). In this study, the y + term, which is known as Prandtl's wall law, is defined as the dimensionless distance normal to the reference temperature. A velocity scale based on the shear stress is applied to the heat flow calculations:

$$q_{wall} = \frac{\rho_f(y_c) \bullet C_{P,f}(y_c) \bullet u_\tau}{T^+\left(y^+_{fluid}\right)} \left(t_{wall} - t_{fluid}\right), \tag{6}$$

$$h_{wall} = \frac{q_{wall}}{\left(t_{wall} - t_{fluid}\right)}. \tag{7}$$

2.3. Influence of mutual radiation when using radiant panels

The calculation of the mutual radiative heat transfer of the radiant panels utilizes Gebhart's absorption coefficient [27]. The absorption coefficient of longwave radiation from surface i to surface j is expressed using equation (8):

$$\beta_{l,j} = F_{l,j}\varepsilon_j + \sum_{k=1}^{J} F_{k\,,\,k}(1 - \varepsilon_k)\beta_{k,j.} \tag{8}$$

The radiation from surface j is determined using equation (9) as follows:

$$ELR_j = \varepsilon_j \sigma T_j^4 - \frac{\sum_{k=1}^{J} \beta_{k,j} \varepsilon_k \sigma T_k^4 S_k}{S_j}. \tag{9}$$

The net radiation emitted by surface j is obtained using equations 10–12 as follows:

$$\sum_{k=1}^{J} \beta_{j,k} = 1, \tag{10}$$

$$\varepsilon_k S_k \beta_{k,j} = \varepsilon_j S_j \beta_{j,k,} \tag{11}$$

$$ELR_j = \varepsilon_j \sigma \sum_{k=1}^{J} \beta_{j,k} \left(T_j^4 - T_k^4\right) = \sum_{k=1}^{J} \beta_{j,k} \alpha_{r,jk} \left(T_j - T_k\right). \tag{12}$$

where the radiant heat transfer coefficient is given by equation (13) as follows:

$$\alpha_{r,jk} = 4\varepsilon_j \sigma \left\{ \frac{\left(T_j + T_k\right)}{2} \right\}^3. \tag{13}$$

The absorption of surface j (ALR_j) is determined using equation (14) as follows:

$$ALR_j = \sum_{c=1}^{C} \frac{\beta_{c,j} LI_c S_c}{S_j} + \sum_{f=1}^{F} \frac{\beta_{f,j} LI_f S_f}{S_j} = \varepsilon_j \left(\sum_{c=1}^{C} \frac{\beta_{j,c} LI_c}{\varepsilon_c} + \sum_{f=1}^{F} \frac{\beta_{j,f} LI_f}{\varepsilon_f} \right). \quad (14)$$

The radiance at surface j (NLRj) is calculated using equation (15) as follows:

$$NLR_j = ELR_j - ALR_j. \quad (15)$$

2.4. Calculation of the heat transfer in radiant panels considering fin efficiency

Fins were introduced between the pipes to prevent an uneven distribution of the surface temperature across the floor surface. Thermal environment of residential buildings (THERB) reproduced heat transport in hot water floor heating by modeling the piping section, hot water in the pipes, and fin section in detail.

Fin efficiency is given by equations (16) and (17).

$$\eta_f = \frac{1}{w} \left[D + (w - D) \frac{tanh \cdot mD}{mD} \right], \quad (16)$$

$$mD = \sqrt{\frac{C_f \cdot P}{\lambda_f \cdot t}} D. \quad (17)$$

The thermal transmittance from the hot water in the pipe to the surface of the pipe is given by equations 18–20:

$$K_p = \frac{A_f}{L_f \cdot R_b}, \quad (18)$$

$$R_b = \frac{D}{\lambda_w \cdot Nu}, \quad (19)$$

$$Nu = \frac{0.0395 \cdot Re^{0.75} \cdot Pr}{1.0 + (1.99 \cdot Re^{-0.125} \cdot (Pr - 1.0))}. \quad (20)$$

Equations 21–23 are the thermal equilibrium equations for the hot water supply.

$$C_w \cdot \rho_w \cdot V_w \frac{\partial T}{\partial t} = \eta_f \cdot K_p \cdot (T_m - T_w) \cdot L_f + Q_s, \quad (21)$$

$$Q_s = q_f \cdot C_w \cdot \rho_w (T_{ws} - T_w), \quad (22)$$

$$-\frac{\partial T}{\partial t} = \eta_f \cdot K_p (T_m - T_w), = \frac{1}{R_m} (T_m - T_{m-1}) + \frac{1}{R_{m+1}} (T_m - T_{m+1}). \quad (23)$$

2.5. Space moisture balance based on air conditioning dehumidification and its effect on power consumption

The heat source model used in this study is based on an equipment characteristics model developed at the Central Research Institute of the Electric Power Industry [23]. A detailed explanation of the model has been provided in previous studies; however, for reference, the equations relevant to this study are listed and explained in this subsection.

The parameters of the equipment characteristic model include the coefficient of performance (COP), power consumption, refrigerant evaporation temperature, refrigerant condensation temperature, outdoor unit blow-off air temperature, and outdoor unit blow-off air relative and absolute humidity values. The dehumidification rate, R [−], which indicates the ratio between the actual and theoretical refrigeration efficiencies, is an input value based on the air conditioner's specifications. The calculation outputs include the power consumption and dehumidification rate.

The refrigerant's evaporation temperature, which is an important parameter used in condensation calculations, is expressed using equation (24):

$$T_{evp,t} = T_{r,t} - \frac{q_t}{M_{evp,t} \bullet C_{a,r,t}}. \quad (24)$$

The refrigerant's evaporation temperature calculated using equation (24) determines if the condensation will occur when the saturated absolute humidity at the refrigerant's evaporation temperature exceeds the absolute humidity of the air in the room at time t. The criterion for condensation is expressed by equation (25):

$$x_{s,evp,t} \leq x_{r,t}. \quad (25)$$

Because the temperature of the heat exchanger surface and the refrigerant evaporation temperature were assumed equal, the saturated absolute humidity, $x_{s,evp,t}$ kg/kg (DA), of the heat exchanger surface and the indoor air absolute humidity were used to

determine the condensation. The dehumidification rate can be calculated as the difference between the inlet and outlet air humidities, as expressed in equation (26):

$$x_{r,remove,t} = x_{r,t} - x_{r,out,t}. \tag{26}$$

The latent heat load is calculated using equation (27):

$$q_{l,t} = 2501 \times M_{r,t} \times x_{r,remove,t}. \tag{27}$$

The total heat load is calculated using equation (28):

$$q_t = q_{l,t} + q_{s,t}. \tag{28}$$

The impact of air-conditioner dehumidification is expressed by equation (29), where the fifth term on the right-hand side represents the dehumidification provided by the air conditioner. The heat load input to the equipment model determines the actual dehumidification rate. The effect of humidification or moisture absorption is represented by the first term on the right-hand side. Other moisture inflows attributed to ventilation or outdoor air is assumed. The latent heat load in equation (27) varies depending on the difference in absolute humidity between blowing and sucking airflows. This is because the relative humidity of the space changes owing to dehumidification caused by the air conditioning, which in turn affects the power consumption. Thus, considering the dehumidification of the radiant panel should improve the accuracy of the calculations.

$$V_{i,ol} \cdot r_{w,i} \frac{d\mu_i}{dt} = \sum_{j=1}^{J} S_{i,j} \cdot \alpha'_{\mu,i,j} \left(\mu_{w,s,j} - \mu_{w,i}\right)\mu_i + \sum_{k=1}^{k} V_k \cdot \left(\gamma_{w,k} \cdot \mu_k^* - \gamma_{w,i} \cdot \mu_i\right) + V_o \left(\gamma_{w,o} \cdot \mu_o^* - \gamma_{w,i} \cdot \mu_i\right) + Q_{g,w} \cdot \mu_i - x_{r,remove,t} M_{r,t}. \tag{29}$$

2.6. Space moisture balance considering radiant panel dehumidification

The moisture balance of the space considering dehumidification by radiant panels is given by equation (30). The fourth term on the right-hand side indicates the dehumidification by the radiant panels. The radiant panel's surface temperature is lower because of cooling by the supplied water, which allows it to reach the dew point temperature. Dehumidification is defined as the moisture potential difference, which is represented based on the laws of thermodynamics and allows the effect of dehumidification to be considered in more detail than in the engineering model (where the water vapor pressure is the driving force of the wet flow) [26].

$$\begin{aligned} V_{i,ol} \cdot r_{w,i} \frac{d\mu_i}{dt} = {} & \sum_{j=1}^{J} S_{i,j} \cdot \alpha'_{\mu,i,j} \left(\mu_{w,s,j} - \mu_{w,i}\right)\mu_i + \sum_{k=1}^{k} V_k \cdot \left(\gamma_{w,k} \cdot \mu_k^* - \gamma_{w,i} \cdot \mu_i\right) + V_o \left(\gamma_{w,o} \cdot \mu_o^* - \gamma_{w,i} \cdot \mu_i\right) + Q_{g,w} \cdot \mu_i \\ & - \sum_{p=1}^{J} S_{i,p} \cdot \alpha'_{\mu,i,p} \left(\mu_{w,s,p} - \mu_{w,i}\right)\mu_i. \end{aligned} \tag{30}$$

2.7. Space heat/moisture balance including air conditioner and radiant panel dehumidification

The indoor humidity balance equation considering the dehumidification provided by both the air conditioner and the radiant panel is given by equation (31) as follows:

$$V_{i,ol} \cdot r_{w,i} \frac{d\mu_i}{dt} = \sum_{k=1}^{k} V_k \cdot \left(\gamma_{w,k} \cdot \mu_k^* - \gamma_{w,i} \cdot \mu_i\right) + V_o \left(\gamma_{w,o} \cdot \mu_o^* - \gamma_{w,i} \cdot \mu_i\right) + Q_{g,w} \cdot \mu_i - \sum_{j=1}^{J} S_{i,j} \cdot \alpha'_{\mu,i,j} \left(\mu_{w,s,j} - \mu_{w,i}\right)\mu_i - x_{r,remove,t} M_{r,t}. \tag{31}$$

The dehumidification terms for the radiant panel use the same equation as the first term on the right side. However, because the surface is cooled and likely to have reached the dew point temperature its effect is considered as subtracting moisture from the space. The accuracy of the power consumption calculation is expected to improve when the dehumidification rates provided by the air conditioner and radiant panel are combined because the heat load input to the equipment characteristic model varies with time. Validating the accuracy of the answer is beyond the scope of this study. The heat balance is given by equation (32):

$$V_{i\,,\,ol} \cdot \overline{c\gamma} \frac{dT_i}{dt} = \sum_{j=1}^{J} S_{i\,,\,j} \cdot \alpha_{c\,,\,i\,,\,j} \left(T_{s\,,\,i\,,\,j} - T_i\right) + \sum_{k=1}^{k} V_k \cdot c\gamma (T_k - T_i) + V_o \cdot c\gamma (T_o - T_i) + Q_{g\,,\,h}. \tag{32}$$

The first term on the right-hand side indicates that the convective heat transfer coefficient is a crucial factor to consider.

2.8. Calculation of power consumption considering dehumidification

The power consumption is expressed in equation (33) as follows:

$$P = P_v + P_c. \tag{33}$$

The actual performance coefficient can be calculated using equation (34):

$$\eta_{tl} = \frac{q}{P_v}. \tag{34}$$

The power consumption of the chiller can be obtained by transforming the actual performance coefficient as follows:

$$P_v = \frac{q}{\eta_{tl}}. \tag{35}$$

The actual performance coefficient can also be expressed as follows:

$$\eta_{tl} = R \bullet \eta_{th.} \tag{36}$$

Substituting equation (36) into equation (35) yields equation (37):

$$P_v = \frac{q}{R \bullet \eta_{th}}. \tag{37}$$

The theoretical efficiency of the refrigeration cycle is expressed by equation (38):

$$\eta_{th} = \frac{T_{evp}}{T_{cnd} - T_{evp}}. \tag{38}$$

2.9. Calculation of the power consumption of radiant panels

The power consumption of the heat source equipment can be calculated using various approaches that employ approximate formulas based on statistical data of the actual usage during floor heating. The power consumption of the heat-pump air conditioning equipment during cooling has not been computed using any method. In this study, the versatility of the equipment characteristic model allowed us to create and extend the algorithm to calculate the power consumption of the heat pump of the heat source equipment using a chilled water generation method. The calculation procedure and flow are described in Section 4. However, the method for deriving the refrigerant evaporation temperature is different. The power consumption of the heat source at maximum and minimum capacities is unknown.

In the equipment characteristic model for air conditioners, the refrigerant evaporation temperature is assumed equal to the surface temperature of the indoor heat exchanger. However, in the case of a radiation panel, as shown in equation (39), the equipment model of the chilled water generator can be obtained by assuming that the refrigerant's evaporation temperature is equal to the return temperature of the circulating liquid. If the return temperature of the circulating liquid has a time-varying value, it can be treated as variable over time in the THERB-side calculation:

$$T_{evp} = T_{w,re}. \tag{39}$$

In the equipment characteristic model, the maximum and minimum cooling capacities (or heating capacity) are required during the calculation. However, using the model when the cooling capacity and power consumption under rated conditions are simply taken from the specifications can lead to inaccuracies. To address this issue, estimated values based on actual measurements were used. For the maximum power consumption, the specification heating values were used. For the minimum condition, the cooling capacity at minimum power consumption according to current measurements was used. Because the cooling capacity of a radiant panel is the amount of heat processed in cooling a liquid, the cooling capacity is expressed using equation (40):

$$Q_L = \left(T_{L,out} - T_{L,re}\right) \bullet L \bullet C_{L.} \tag{40}$$

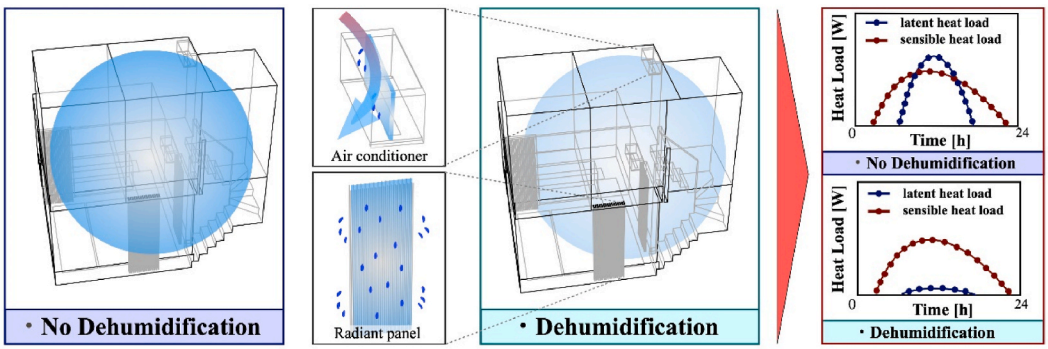

Fig. 2. Proposed coupled analysis methodology.

3. Materials and methods

3.1. Incorporation of air-conditioner dehumidification model into THERB

As this study is an extension of a previous study [20], detailed explanations are omitted herein. The analysis in this study used the THERB tool for heat–air–moisture (HAM) analysis. THERB is a dynamic and highly versatile heat load simulation tool that enables combined heat and moisture transfer[8]. It is widely used for various thermal environment simulations and power consumption calculations [23].

The proposed analysis tools can be used to calculate the power consumption and dehumidification of radiation panels. Although previous studies have focused on the dehumidification and power consumption of air conditioners [23], they did not consider the coupled convective heat transfer coefficient. Therefore, a novel model that includes both air conditioning and radiant panels was incorporated into THERB for HAM analysis.

Fig. 2 shows the latent heat load variation with and without dehumidification. It must be noted that Fig. 1 shows only a conceptual diagram based on the hypothesis that the latent heat load varies and does not imply that dehumidification significantly affects power consumption. Yamamoto et al. [23] already confirmed the effect of air-conditioner dehumidification on the latent heat load in a previous study. Dehumidification was incorporated into the generic equipment characteristic model developed by the Central Research Institute of the Electric Power Industry for air conditioners. The accuracy of the power consumption calculation was found to

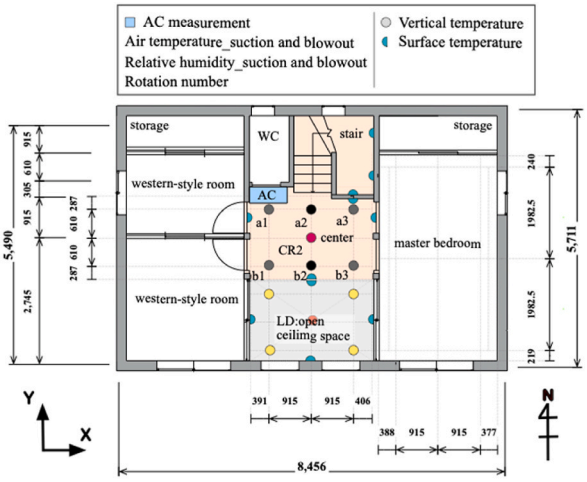

(a) 1F plan and experimental measurement points

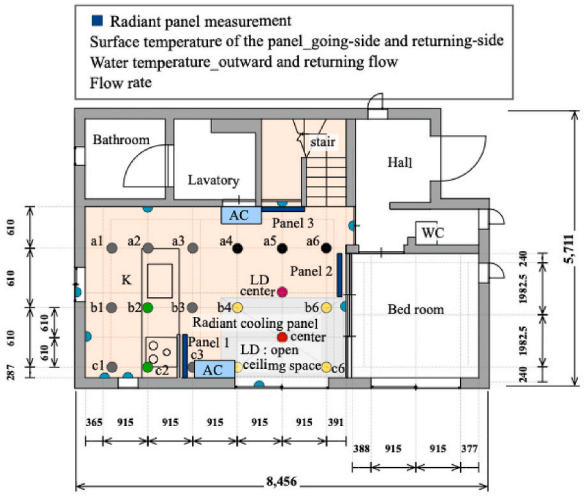

(b) 2F plan and experimental measurement points

Fig. 3. Plan views of the experimental house and measurement points (Yamamoto et al. [20]).

be affected when the dehumidification rates were not coupled, compared to the case where the relative humidity was a constant value [23]. Therefore, in this study, a coupled dehumidification system was implemented to decrease the previously calculated dehumidification amount in subsequent calculations, with the aim of improving accuracy. Such a system was incorporated in the current study.

The power consumption of the air conditioner was expected to be significantly affected by the variation in the latent heat load, which was derived from the difference between the amount of dehumidification provided by the equipment and the space moisture balance. To improve accuracy the chilled water piped radiant air conditioning system in THERB was extended to consider fin efficiency when calculating the dehumidification provided by radiant panels. Based on the moisture potential theory developed by Ozaki et al. [26], fin efficiency is defined as the ratio between the net heat transferred from the fin surface and the heat transferred assuming the hot water temperature is equal to the total surface temperature of the fin. The effect of dehumidification is considered when calculating the space moisture balance. The effect of incorporating the dehumidification provided by the equipment on the accuracy of the verification results was evaluated and an operation technique that considered the effect of dehumidification and satisfied both energy efficiency and comfort was developed using case studies.

3.2. Outline of the subject building

The accuracy of the building model was verified using the equipment model, and that of power consumption of the radiant panels was verified using test data [24] from an experimental house built in an artificial weather chamber. Fig. 3 shows plan views of the experimental house and measurement points. The kitchen, living room, staircase on the first floor, hallway on the second floor, and atrium were analyzed (orange portions in Fig. 3; the measured heights differ for each color). Please refer to previous studies for data not used in this study [20].

The ceiling heights of the first and second floors were 2400 mm from the FL. The height from the FL of the living room to the ceiling of the atrium space was 5290 mm. Three convection air conditioners (hereafter referred to as "air conditioners") were installed in the experimental house: one on the second floor, and the other two on the first floor. Radiant air conditioning (hereafter referred to as "radiant panels") was turned off in rooms other than those analyzed during the actual measurements. Three radiant panels were installed on the first floor of the experimental house. The surface temperature of the panels, as well as the onward and return temperatures and flow rate of the circulating fluid, were measured to determine the heat input (the onward and return temperatures of the circulating fluid were already published in Yamamoto et al. [24]). These data were measured on three radiation panels. All the temperatures were measured using T-type thermocouples with a precision of ± 0.5 °C.

The experimental house was designed to meet the ZEH standard (energy-saving regional category 4–7, UA = 0.6 W/m^{2}K) [20]; therefore, it exhibited sufficient thermal insulation performance. The building was steel-framed with 75-mm-thick lightweight concrete exterior walls. Therefore, a case study on the combined use of radiant panels and air conditioners, which have been increasingly used in buildings with adequate thermal insulation performance, could prove advantageous.

The radiation panels used in this study consisted of cross-linked polyethylene pipes sandwiched between aluminum plates. The connection was made of resin and the structure was treated to provide high durability against rust and corrosion. A total of 10 or more aluminum plates were used to create a single panel (W850 × D100 × H2,400 [mm]). The radiant panels used a common water-cooled heat pump as the heat source.

3.3. Measurements and test conditions

Details of the experimental conditions and the equipment specifications used in the study are provided in Yamamoto et al. [20]. Table 1 provides a summary of the most relevant experimental conditions.

4. Verification of accuracy of dehumidification models and power consumption of radiant panels

The accuracy of the power consumption estimation model that incorporated dehumidification was verified based on the results of an experiment conducted by Yamamoto et al. [20]. Measured values of the blowout, intake temperature, and humidity were used. In this section, we examine the extent to which the space relative and absolute humidities are affected when space dehumidification with air conditioners and radiant panels is considered. Further, the degree of its influence on PMV is also validated.

Table 1
Experimental conditions [20].

Target	Item	Conditions
Artificial weather chamber	Set temperature	35 °C
	Set chamber humidity	60%
	Ventilation frequency	0.7 times/h
Air conditioning	Set temperature	28 °C
	Blowout angle	0° (From a horizontal plane)
	Wind speed	Weak operation
Radiant panel	Set temperature	24 °C

4.1. Verification of accuracy of radiant panel models

The accuracy of the radiant panel model was validated. Figs. 4(a)–(c) show the results of the verification of the accuracy of the radiant panel's surface temperature. The measured outward temperature was used as the input. In addition, the flow rate varied over time following the actual measured flow rate reported by Yamamoto et al. [20], which was in the range of 1.8–2 L/min. In the case study, specification values were used as fixed values. The surface temperature of Panel 1 (Fig. 4(a)) was lower than the calculated value, which could be attributed to local variations in the air temperature near Panel 1 or the connection between the radiant panels being remarkably complicated. Only Panel 1 was constantly used by the control system. The remote-control units, which served as sensors, were accurately located. Because Panel 1 was located near the window, the local temperature may have been higher. THERB used the bulk temperature as the reference temperature, and the error was considered to have occurred within that range. There were various possible sources for the error in Panel 1, including the measurement device (±2.5 °C) or the position of the panel's sensor. Such errors could occur because the panel's sensors were concentrated in one location. Because these errors were within the error ranges of the measuring instruments, the sensors were considered to provide accurate values. Yamamoto et al. showed that the effect of a

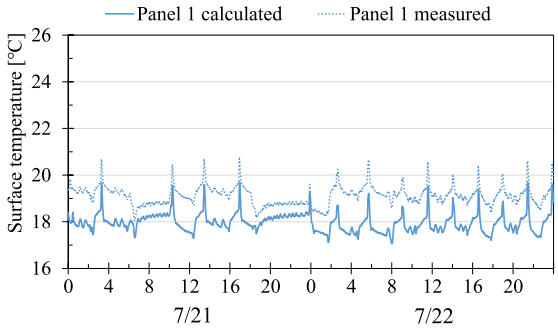

(a) Accuracy verification results for the surface temperature of Panel 1

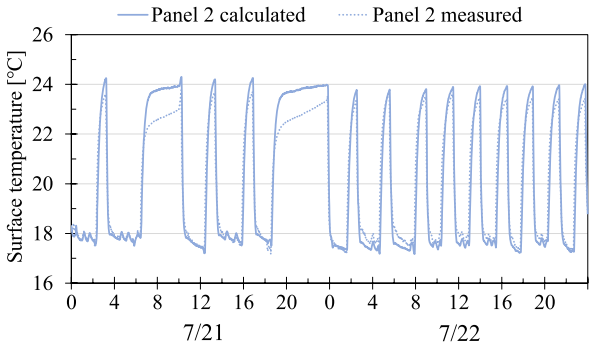

(b) Accuracy verification results for the surface temperature of Panel 2

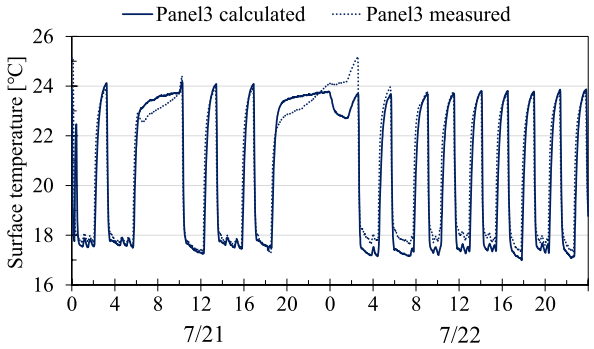

(c) Accuracy verification results for the surface temperature of Panel 3

Fig. 4. Accuracy verification results for the surface temperatures of the radiant panels [20].

difference in surface temperature was small for the calorimetric diffusion coefficient, and therefore, the error was acceptable [20]. The effect of the surface temperature on the thermal diffusivity was small because the surface temperature was not used in the thermal diffusivity formula. In other words, the surface temperature had little influence because the effect of the heat loss was dominant. Although the surface temperature contributed to the heat loss, it was considered part of the heat loss.

In addition, because this was a relative comparison, the reference temperatures were expected to vary because the air conditioner was operating on the first floor. Therefore, no adjustment factor was used. Some errors in the radiation calculations were expected because of differences in various factors such as the form factor. The errors are considered acceptable here because the primary purpose of this section is to draw relative comparisons based on case studies. The control issue that resulted in only Panel 1 operating during the accuracy verification process is unresolved. Panels 1 and 3 (Fig. 4(c)) were used in Case 2 but not in Case 3 because Panels 2 (Fig. 4(b)) and 3 were too close for practical simultaneous operations; it was necessary to operate Panels 1 and 3 simultaneously.

4.2. Verification accuracy of power consumption of air conditioners and radiant panels

The accuracy verification was intended to be complementary. Even if there was a quantitative error of some percentage, the actual measured power consumption followed the same trend, and therefore, considering the purpose of this study, there was no need to issue an MAPE. The power consumption trend repeated itself in every operation, but its validity could not be determined, especially for radiant panels. Furthermore, the case study assumed a convective heat transfer coefficient of 4 W/m^{2}K, which was a relative

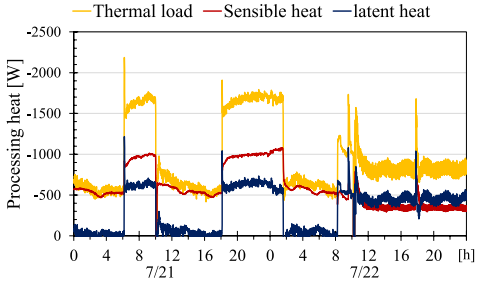

(a) Processed heat input for the air conditioner equipment model

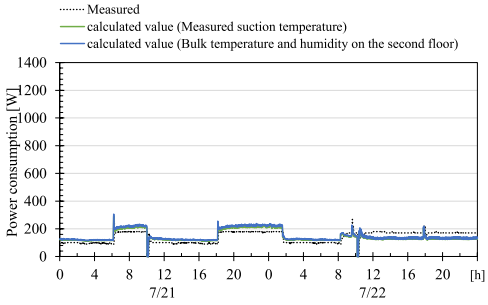

(b) Accuracy verification of the air conditioner energy consumption

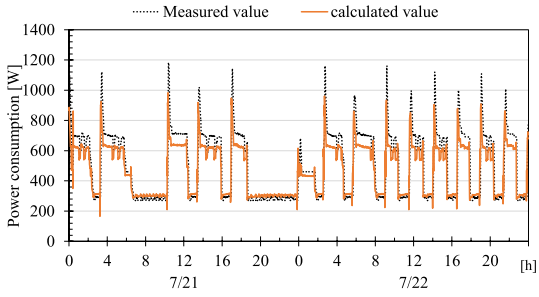

(c) Accuracy verification of the power consumption of radiant panels

Fig. 5. Accuracy verification results for the power consumption of air conditioners and radiant panels.

comparison. A simple comparison is sufficient for verifying accuracy in relative studies.

The equipment characteristic model used dehumidification when computing the power consumption; therefore, the validity of the dehumidification coupling was confirmed by verifying the accuracy of the power consumption; this helped verify the actual measurement results. Fig. 5(a) shows the equipment model heat input process. The sensible heat loads are given by equation (41):

$$Q_S = (T_{ein} - T_{eout}) \bullet M_{in} \bullet C_a \bullet \rho_a, \tag{41}$$

where Q_s, T_{ein}, and T_{eout} represent the actual measured sensible heat load [W], inlet temperature [K], and outlet temperature [K], respectively.

The latent heat load is given by equation (42):

$$Q_L = (X_{ein} - X_{eout}) \bullet M_{in} \bullet C_a \bullet \rho_w. \tag{42}$$

The sensible and latent heat appeared to respond in a step-controlled manner because the radiant panels were turned off while the air conditioner produced no sensible heat. This increased the amount of heat being processed. Fig. 5(b) shows the results of the verification of the accuracy of the air conditioner's power consumption. The actual measured values exhibited a step change in the 100 W–180 W range for the load. The case where the bulk temperature and humidity of the second floor were used as input values for the equipment model was compared with the scenario where the measured intake temperature and humidity of the actual air conditioner were used. The results showed that the power consumption corresponded to the actual measured values when the actual measured intake temperature was used as the reference temperature. This could be attributed to the rise in refrigerant evaporation temperature with the suction temperature. However, the prediction accuracy was validated, even when the bulk temperature and humidity of the second floor were used as inputs. The suction temperature significantly affected the refrigerant evaporation temperature; therefore,

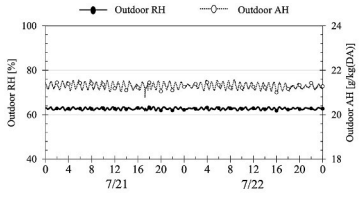

(a) Experimental conditions for outdoor relative and absolute humidities

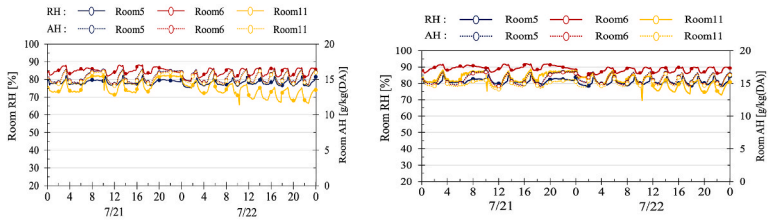

(b) Relative and absolute humidity change over time when dehumidification is considered

(left: coupled convective heat transfer coefficient; right: 4 W/m^{2}K)

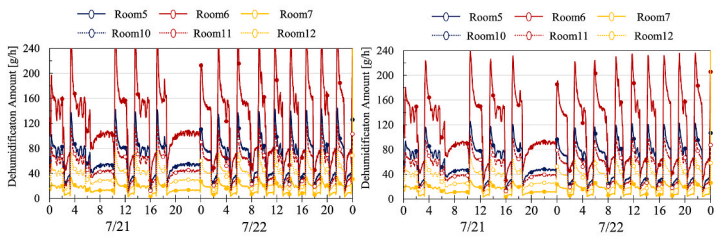

(c) Dehumidification in each zone of THERB

(left: coupled convective heat transfer coefficient; right: 4 W/m^{2}K)

Fig. 6. Environmental humidity and dehumidification rate in each zone when considering dehumidification (with and without convective heat transfer coefficient coupling).

caution should be used in flow fields where local temperature stratification occurs. Fig. 5(c) shows the results of the accuracy verification of the radiant panel power consumption. The calculated values were tracked, and the measured values were consistent during the operation of the radiant panel. Although the measured outgoing and returning temperatures were used as input conditions, the low measurement accuracy of ±2.5 °C for the measured return temperature affected the accuracy of the power consumption calculation. However, the calculation accuracy was high when one unit was in operation. Using specification values during heating affected the calculation accuracy for the maximum power consumed.

4.3. Impact of considering dehumidification on a humid environment

Figs. 6(a)–(c) depict the level of dehumidification in each zone of a humid environment when dehumidification is considered. During the accuracy verification, dehumidification was considered under the following conditions (Fig. 6(a)). Dehumidification was considered in Step 5 in the analysis flow. The relative humidity of the outside air, absolute humidity, and relative humidity were approximately 63%, 21 kg/kg (DA), and 70%–80%, respectively. The maximum dehumidification rate in Room 6, where the radiation panels were installed, was 240 g/h (Fig. 6(c)). This relatively high dehumidification rate was the cause of the low relative humidity in Room 5 (Fig. 6(b)). The dehumidification process should be considered because the relative humidity depends on the volume of the space. ESs often uses customary values for indoor relative humidity. In this study, the indoor humidity was set at 70% (Fig. 6(a)). The environmental humidity and dehumidification rate, when the customary value of 4 W/m^{2}K is given as the boundary condition for the THERB wall surface, were discussed. In Room 11 on the second floor both, the relative and absolute humidities were found to be higher than the room temperature calculated using the convective heat transfer coefficient obtained from CFD. This difference was attributed to the lower calculated room temperature. In contrast, the relative humidity showed a high value of approximately 80%, indicating a need for dehumidification in this environment.

4.4. Dehumidification of air conditioners and radiant panels with and without coupled convective heat transfer coefficients

Figs. 7(a) and (b) show the heat values of the processed heat rate and dehumidification of the equipment during the 4 W/m^{2}K coupling. The high load periods for the air conditioner processed heat rate and the dehumidification of the radiant panel were closely correlated Fig. 7(a). The accuracy of the proposed method was examined based on the experimental data from the previous study [24]. The convective heat transfer coefficient of the wall surface is important when using the equipment characteristic model. However, this is not expected to raise significant issues when used for relative comparisons. Because there were no errors in the calculation of the room temperature, there was no variation in the level of dehumidification provided by the radiant panel. The degree of dehumidification provided by the radiant panel was caused by condensation as the refrigerant evaporation temperature fell and the heat load

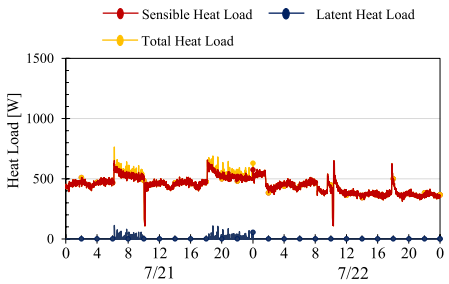

(a) Processed heat of air conditioner when calculated at 4 W/m^{2}K

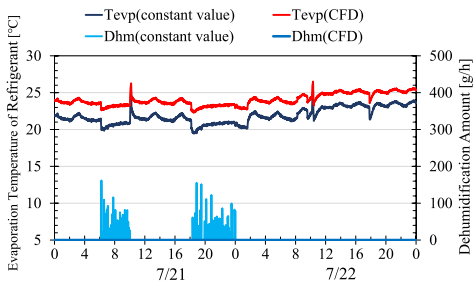

(b) Dehumidification of air conditioner calculated at 4 W/m^{2}K

Fig. 7. Processed heat and dehumidification of equipment at 4 W/m^{2}K.

increased during the day (Fig. 7(b)). The dehumidification provided by the air conditioner occurred during periods of low refrigerant evaporation temperatures.

4.5. Comparison of results for calculating the frequency of PMV occurrence

Fig. 8 shows the frequency of occurrence of PMV with and without dehumidification. Although there was no considerable difference in the overall trends (Figs. 8(a) and (b)), the PMV of Room 5 moved closer to the median when dehumidification was not considered (Fig. 8(b)). This was because the PMV remained at approximately 75% when dehumidification was considered (Fig. 8(a)), which resulted in a low PMV value. The conditions during the accuracy verification indicated that considering dehumidification enables safe evaluation. The rate and number of PMV occurrences should be examined when the accuracy of the building model and power consumption has been verified. It was possible to draw some conclusions regarding the relative evaluation in the case study because this demonstrated the value of dehumidification coupling.

5. Proposal for optimal operation using both air conditioning and radiant panels

5.1. Purpose of the case study

As described in the previous section, we verified the accuracy of the calculation of power consumption of the air conditioners and radiant panels and evaluated the effect of dehumidification. The aim of this case study was to propose an operating strategy for air conditioners and radiant panels that balances comfort and energy efficiency while considering the dehumidification provided by the air conditioners and radiant panels in the calculations.

To this end, algorithms for the dehumidification provided by the air conditioners and radiant panels were incorporated and extended to an analytical tool that tracks humidity fluctuations over time. The power consumption of the air conditioners and radiant

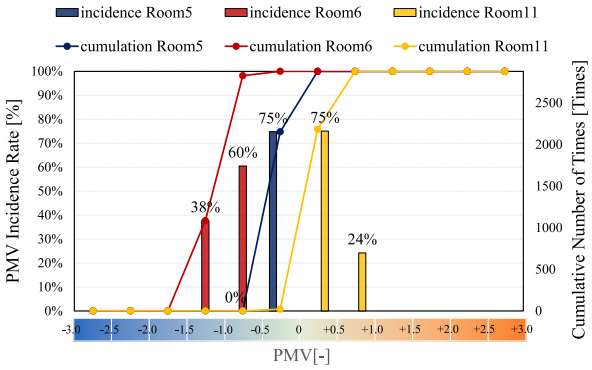

(a) PMV occurrence rate with dehumidification

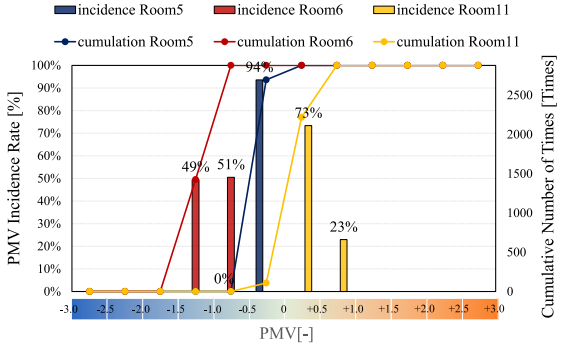

(b) PMV occurrence rate without dehumidification

Fig. 8. Frequency of PMV with and without dehumidification (over 2 days).

panels was calculated using the equipment characteristic model developed by the Central Research Institute of Electric Power [24]. The contribution of the power consumption of the air conditioners and radiant panels to the PMV (i.e., the comfort index) was also calculated.

5.2. Case study details

Table 2 lists the details of this case study. The number of panels and the location of the air conditioner were used as variables to establish representative cases. The water supply temperature was varied between 7 and 15 °C to verify the panels' sensitivity to the impact of their capacity. The parameters were varied to determine an optimal operation strategy for air conditioners and radiant panels operating together in a large area. The calculation of the heat diffusion coefficient based on the on/off status of the radiant panels did not affect the results. Therefore, in this study, the water supply temperature for Cases 1–4 was set to 7 °C. The analysis used the heat diffusion coefficients of Cases 1-1, 2-1, and 3-1 at water supply temperatures of 7 °C and 15 °C. In the case studies, the heat input of the air conditioner was set to a "low" operating condition during the accuracy verification.

Our focus in this study was on achieving both comfort and energy efficiency when supplementing the radiant panels with air conditioners. The air conditioner was not operated at "high" level to avoid highly irregular temperature distributions. This study was conducted using a highly insulated house that was equivalent to the ZEH as buildings complying with the revised law are often highly insulated and in high demand.

A typical analysis workstation would take approximately four days to complete the analysis; therefore, it was not suitable for investigating numerous cases. The proposed method anticipates future improvements in computing power (the use of supercomputers and the development of quantum computers). However, this study used an optimal operation scheme with the proposed method.

5.3. Method and assumptions for setting boundary conditions

Yamamoto et al. [24] used measured values to calculate many CFD boundary conditions. Therefore, some analytical errors needed to be accepted. For a relative evaluation, the convective heat transfer coefficient was set to 4 W/m^{2}K. The measured values were not tracked despite the building model's validity being guaranteed within a given range owing to the variations in the convective heat transfer coefficient's reference temperature for the locations where some temperature stratification occurred. This may be an ES-specific problem and is, therefore, beyond the scope of this study. However, it is believed that the determination of the optimal operation method for air conditioners and radiant panels were not significantly affected because the evaluation was relative and the calculation results were used as reference values during the accuracy verification process.

The measured air conditioner blowout temperature and airflow rate were used as boundary conditions for the CFD model. The rated value was used as the air volume with respect to the airspeed. The blowout temperature was derived through a convergence process based on the THERB heat load calculated using equation (43):

$$q_t = v \bullet \gamma \bullet A_{air}(T_{air} - T_{su}) \tag{43}$$

Fig. 9 shows the flow of the analysis after it was modified based on the accuracy verification process. The wall surface temperature and heat load were calculated in Step 1 and then used in Step 2. These changes were made after carefully analyzing the computational load and available time. Therefore, during the accuracy verification process, the measured values were monitored within a specific range even when the convective heat transfer coefficient was set to a standard value of 4 W/m^{2}K.

5.4. Comfort prediction and discussion of results

Table 3 lists the conditions used for the PMV computations. Light summer clothing was assumed for the calculations. The room

Table 2
Case study details.

Case		Radiant panel conditions			AC units in operation
		Radiant panel	Water temperature [°C]	Flow rate [L/min]	
		Number of units in operation			
Case 1	Case 1-1	3 units	7		2FAC
	Case 1-2		11		
	Case 1-3		15		
Case 2	Case 2-1	2 units	7		2FAC
	Case 2-2	(Panels 1 and 3)	11		
	Case 2-3		15	1.5	
Case 3	Case 3-1	1 unit	7		2FAC
	Case 3-2	(Panel 3)	11		
	Case 3-3		15		
Case 4	Case 4-1		7		1FAC
	Case 4-2		11		
	Case 4-3		15		

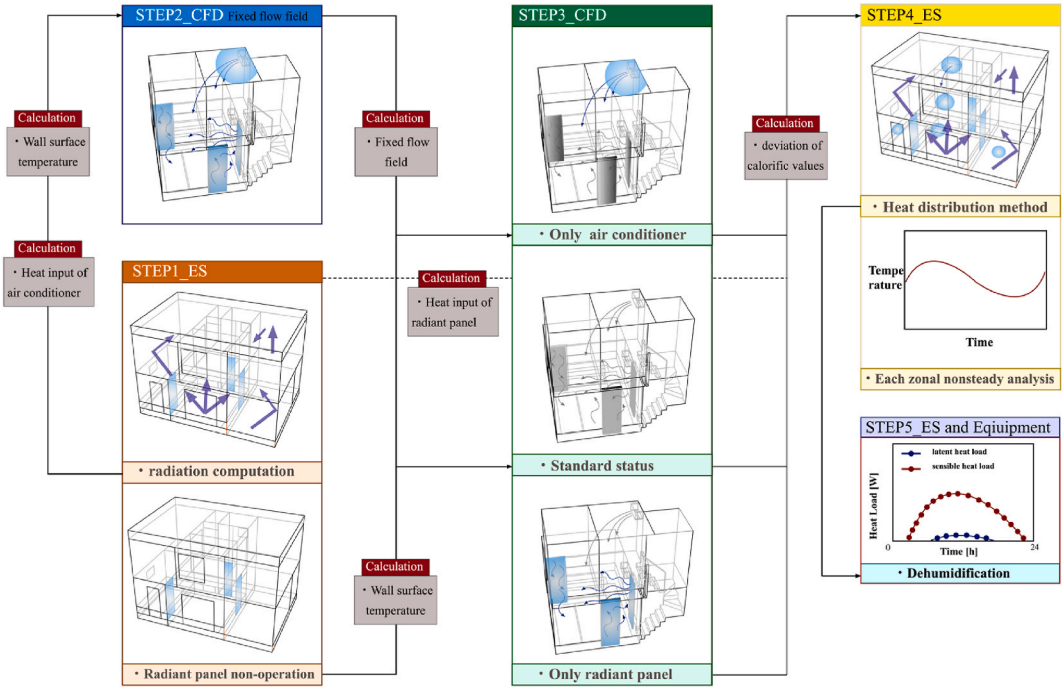

Fig. 9. Analysis flow using only the values calculated for the proposed method.

Table 3
PMV calculation conditions.

Item	Condition
Air temperature	THERB-calculated value
Relative humidity	THERB-calculated value
Airflow (wind speed)	CFD-calculated value
Average radiant temperature	THERB-calculated value
Amount of clothing	0.5 [clo]
Metabolic rate	1.0 [met]

temperature and relative humidity are easy-to-understand indicators for evaluating PMV; however, individual preferences can vary. Therefore, in this study, the comfort evaluation was based on the PMV specified in ISO-7730 [28]. Meteorological data from the standard year of the extended AMeDAS were used to ensure the generality of the case study. Table 4 shows the analysis conditions for THERB. Because this is a relative comparison, convective heat transfer coefficient of 4 [W/m^{2}K] was used, which is the customary value. Table 5 lists the analytical conditions for the CFD used in Step 2 (Fig. 9). A low-Re-type k-ε model was used for the turbulence because it was adapted to the analysis conditions during the accuracy validation. The conditions set here were aligned with those set during the accuracy verification process. The air conditioner blowout velocities were rounded to the nearest values used during the

Table 4
THERB analysis conditions.

Item	Condition
Computation period	7/20–25
Computed time interval	1 min
Building location	Tokyo metropolitan area
Building azimuth	South
Weather data	Tokyo Standard Year Extended AMeDAS (2001–2010)
Ventilation frequency	0.7 [Time/h]
People in the room	None
Convective heat transfer coefficient	4.0 [W/m^{2}K]
Relative humidity	By air conditioner Calculated taking dehumidification into account (There is also a comparison with no dehumidification)
Number of days for preliminary calculation	5 [days]
Set temperature for Step 1	25 [°C]

Table 5
Analysis conditions for CFD in Step 2.

Item	Condition			
CFD code	STAR-CCM+ 12.04.011			
Turbulence model	Standard low-Re k–ε model			
Number of meshes	Approx. 5 million (adjusted on a case-by-case basis) $y+ > 1$			
Wall boundary condition	Enter the calculated value of THERB in step 1 [°C]			
	Velocity: no-slip, $k|_{wall}$: no-slip			
	K: von Karman's constant [−]			
Air supply port	L_{AC}: 0.088 [m]			
	L_{vent}: 0.0075 [m] v: wind speed [m/s]			
	C_μ: model coefficient [−] k: kinetic energy [m^2/s^2]			
	I: turbulence intensity [−]			
	ε: turbulence dispersion rate [m^2/s^3]			
Inflow boundary	Turbulence Strength		Air conditioning	0.05 [−]
			Ventilation opening	0.01 [−]
	Ventilation opening	Inflow temperature	All cases	34.18 [°C]
		Flow rate		0.018 [kg/s]
	Blow-off flow rate			0.105 [kg/s]
	Air conditioning	Angles		0 [°] (horizontal level)
	Blast temperature		Case 1	Air conditioner 20.4 [°C] Ventilation opening 35.4 [°C]
			Case 2	Air conditioner 20.15 [°C] Ventilation opening 35.4 [°C]
			Case 3	Air conditioner 20.32 [°C] Ventilation opening 35.4 [°C]
			Case 4	Air conditioner 16.85 [°C] Ventilation opening 35.4 [°C]
	Air conditioner: Intake		All cases	0.105 [kg/s]
	Gas exchange port: export realm			0.018 [kg/s]

accuracy verification to conduct a relative evaluation based on a case study that captured an actual situation rather than using the rated value, which could cause excessive cooling according to the accuracy verification results. Here, the condition $y+ > 1$ was generally satisfied. Further, u+ and y+ were expressed as linear relationships for the near-wall treatment. However, even in the few scenarios where $y+ < 1, 1.5 > y+$ was satisfied. Therefore, the accuracy was not significantly impaired and the analysis was considered acceptable because its purpose was to conduct a relative evaluation. The blowout temperature of the air conditioner in Case 4 was lower than those in the other cases because of the strong solar radiation load from the window on the first floor.

5.4.1. *Typicality of outdoor air temperature*

Fig. 10 shows the fluctuations of the relative humidity and temperature of the outdoor air. The hottest days with highs exceeding 35 °C were used. A typical day in summer has a relative humidity ranging from 50% to 80%. The extended AMeDAS weather data were used from preliminary calculations to ensure the representativeness of the analysis.

5.4.2. *Comparison of heat input for integration*

Fig. 11 shows the heat input of the air conditioners and radiant panels for each case investigated over two days (July 24–25). There was no change in heat input with or without dehumidification because the heat load in Step 1 was used, and no dehumidification was performed. If dehumidification is performed, it is closely related to the calculation method for the air conditioner input, which implies that boundary conditions are calculated using the equipment characteristic model. Dehumidification was ignored in the heat input computations used in this study because such estimation was considered esoteric owing to the need for a stepwise preliminary investigation. The latent heat was not calculated in Step 1 because the sensible heat load should be used as the heat input for the proposed method. When three panels were used, the radiant panel showed a value of approximately −1290 kJ, which was approximately 1.74 times higher than that of the air conditioner. In Case 4, the heat input of the air conditioner was a large value, approximately −1095 kJ. Compared to Case 3, which had the same number of panels (one panel) the heat input was higher. This was because

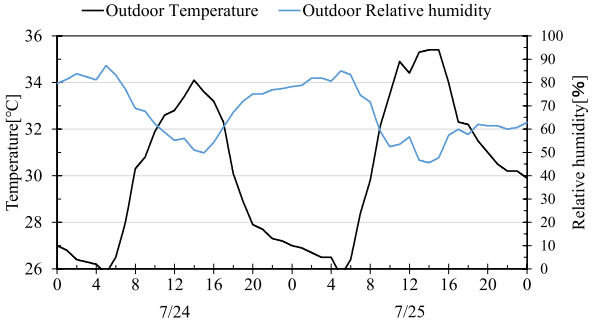

Fig. 10. Change in relative humidity and temperature of the outside air.

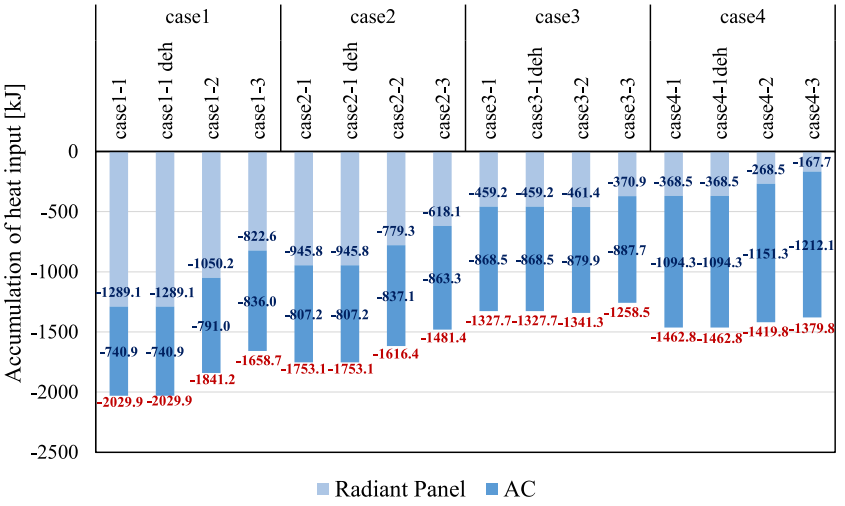

Fig. 11. Comparison of heat input over two days (July 24–25) for air conditioners and radiant panels.

the amount of heat input for the radiant panels depended on the chilled water supply (water temperature and flow rate). Even if the input heat did not change significantly, the amount of heat processed on the first floor could be high because of the increased heat from the solar radiation through the windows. For Cases 1–3, the heat input from the air conditioner was based on the second-floor data; for Case 4, it was based on the first-floor data. Although these features are debatable, they were not discussed in this study because it was a relative comparison.

5.4.3. Comparison of calorimetric diffusion coefficients

Fig. 12 shows the heat diffusion coefficients for each investigated case. The air conditioners were mostly confined to the second floor, with a value of approximately 0.75–0.8 [-] for the two floors. In contrast, the radiant panels distributed approximately 0.75 [-] of the heat for the first floor combined, which was equivalent to convection. When using a reduced number of panels, the heat diffusion showed a marginal difference, whereas Case 4 distributed approximately 0.68 [−] of the heat compared to that in Room 6. The panel surface temperature had little effect on the heat distribution coefficient. Therefore, convection will have a greater effect on the heat loss than the surface temperature. In this case study, only Case 4 considered the condition where the forced convection field fluctuated. However, validating the sensitivity of the radiant panel is a priority based on the actual operational conditions. In the future, it is necessary to investigate its compatibility with the actual operation of air conditioners; however, it should be emphasized that humans find forced convection fields uncomfortable because of the draft effect.

5.4.4. Comparison of the accumulated dehumidification provided by air conditioners and radiant panels

Fig. 13(a) and (b) shows the dehumidification provided by the air conditioner and the total dehumidification provided by the air conditioner and radiant panels in two days. The highest dehumidification was observed when three panels were in operation (Fig. 13 (a)). The dehumidification decreased with the number of panels. Further, it decreased with an increase in the temperature of the water supply. This was because the panel surface temperature increased, and no condensation occurred. The air conditioner dehumidified in Case 4, but the dehumidification rate was lower at 302.63 kg/h even when the temperature at which the radiant panel was pumped was the same as that in Case 3-1. In this case, the air conditioner dehumidified at 68.49 kg/h, for a total dehumidification of 371.12 kg/h. In Case 4, the dehumidification rate of the air conditioner increased with the water supply temperature. This was because the air

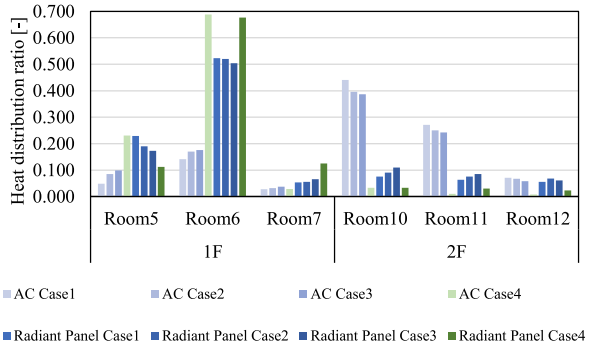

Fig. 12. Heat quantity diffusion coefficients for each case.

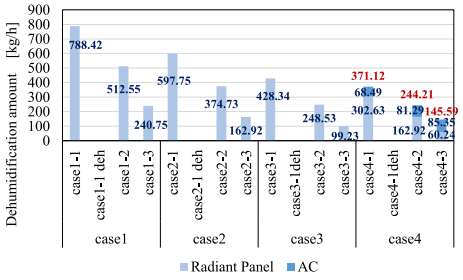

(a) Total dehumidification of air conditioner and radiant panel over 2 days

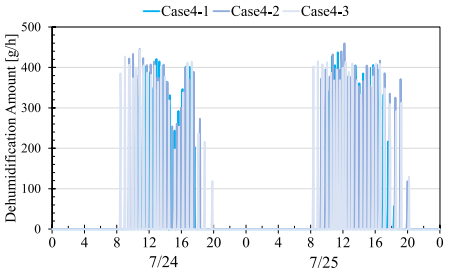

(b) Change over time in air-conditioner dehumidification (Case 4)

Fig. 13. Total and air-conditioner dehumidification over 2 days.

conditioner compensated for the lack of dehumidification by the radiation panel. Dehumidification occurred during daytime hours (approximately 8:00 to 18:00) according to variations in the air-conditioner dehumidification over time (Fig. 13(b)). This was most likely caused by the increased heat load from solar radiation transmitted through the window.

5.5. Contribution to indoor temperature and environmental humidity by applying the proposed method for air conditioners and radiant panels

We assessed the relative PMV and power consumption of each zone when air conditioners and radiant panels were used together. The latter was assessed using the total power consumption for two days to match the comparison method for the PMV and power consumption. The ratio of the space volume determined the amount of dehumidification by the radiant panels.

5.5.1. Comparison of representative cases with and without dehumidification provided by air conditioners and radiant panels

Cases 1-1, 2-1, 3-1, and 4-1 were used to compare the air conditioners and radiant panels with and without dehumidification. A water supply temperature of 7 °C was selected because it was within the acceptable range for the accuracy verification and required little power. Additionally, it was used to determine the influence of the amount of electricity consumed by the air conditioner.

5.5.1.1. Comparison of representative cases 1 to 4 (water supply temperature 7 °C). Fig. 14 shows the occurrence rate and frequency of PMV in the case studies. In Case 4, the first floor shows the median value of the PMV; however, the second floor shows a higher value and is outside the comfort range because no equipment is installed on the second floor. In contrast, the corridor on the second floor may be used on the first floor, but it is beyond the range of the air conditioning system. However, this study could only present possibilities because the PMV would depend on actual usage.

5.5.1.2. Sensitivity analysis of water supply temperature for radiant panels in cases 1 to 4. In Case 1, the PMV value approached the median value with an increase in the water supply temperature; a similar trend was observed in Case 2. In Case 4, an increase in the water supply temperature did not affect the second floor; however, the first floor showed values of −0.5 [−] to 1.0 [−] when the water supply temperature was 7 °C. The first floor showed a high frequency of values occurring in stages that were close to the median value when the water supply temperature was increased to 15 °C.

5.5.1.3. Comparison of the impact of dehumidification in representative Cases 1 to 4 (water supply temperature of 7 °C). Case 1-1 (no dehumidification) to Case 4-1 (no dehumidification) (Figs. 14 (b),(f),(i),(n))represent the cases with no dehumidification. Compared to

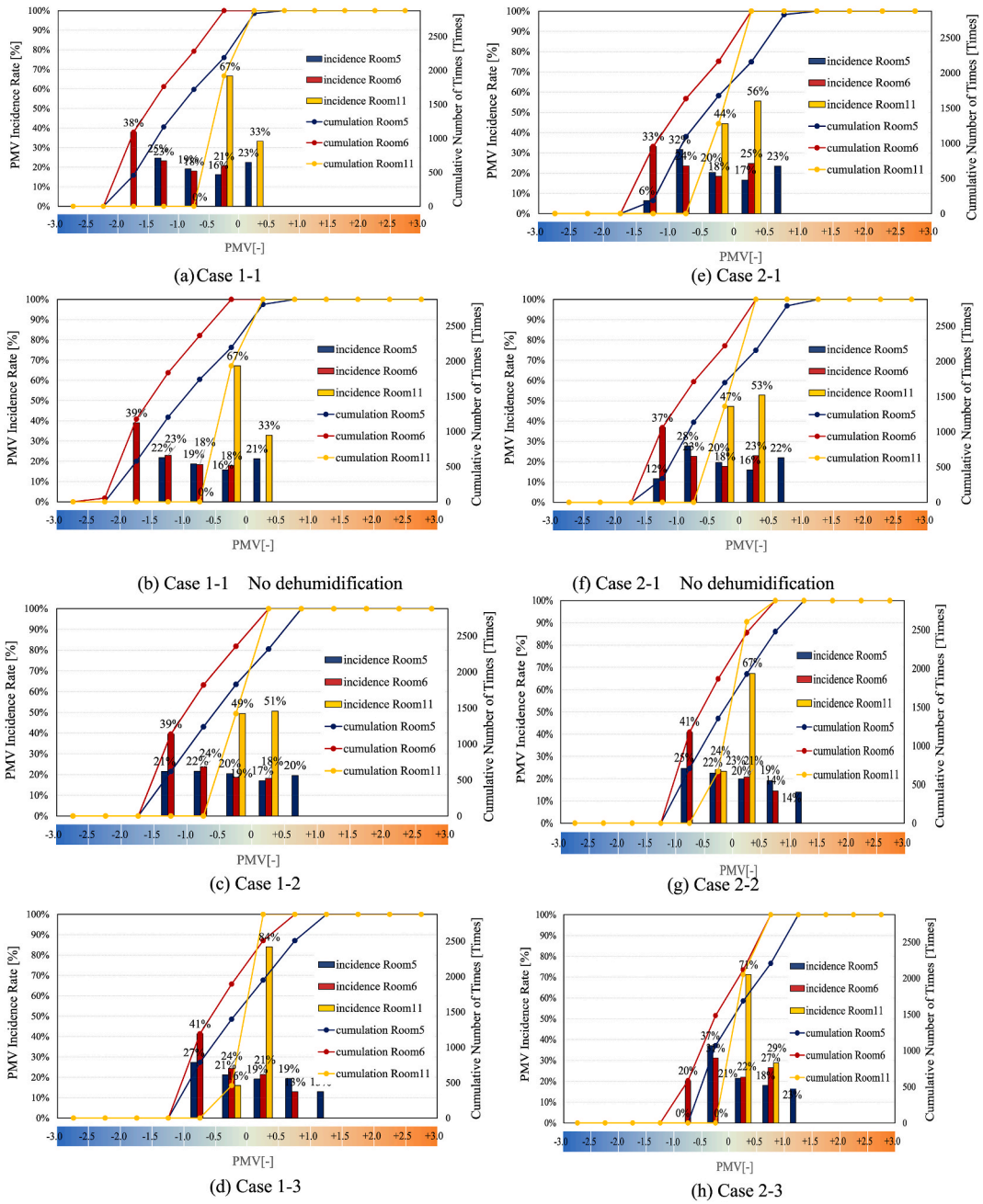

Fig. 14. Percentages and numbers of PMVs in the case studies.

Case 1(Fig. 14 (a)), with and without dehumidification, there was only a small error (Figs. 14 (a)–(p)). The first floor showed a small difference, but the second floor showed no variation. This was because of the lack of dehumidification by the air conditioners. Thus, dehumidification had a minimal impact on the radiant panel. In Case 2, the effect of dehumidification on the PMV on the first floor was approximately 4% at the maximum, which indicated that dehumidification had a significant effect (Figs. 14 (e),(g),(h)). In addition, the effect of dehumidification on the second floor was approximately 3% because of the higher impact of the radiant panels on dehumidification. Dehumidification by the air conditioners was only observed in Case 4 (Figs. 14 (m),(o),(p)). In Case 3, the PMV rate on the second floor was 7% higher than with no dehumidification (Figs. 14 (i),(k),(l)). The effect of the dehumidification by the radiant panels fluctuated with a decrease in the number of panels.

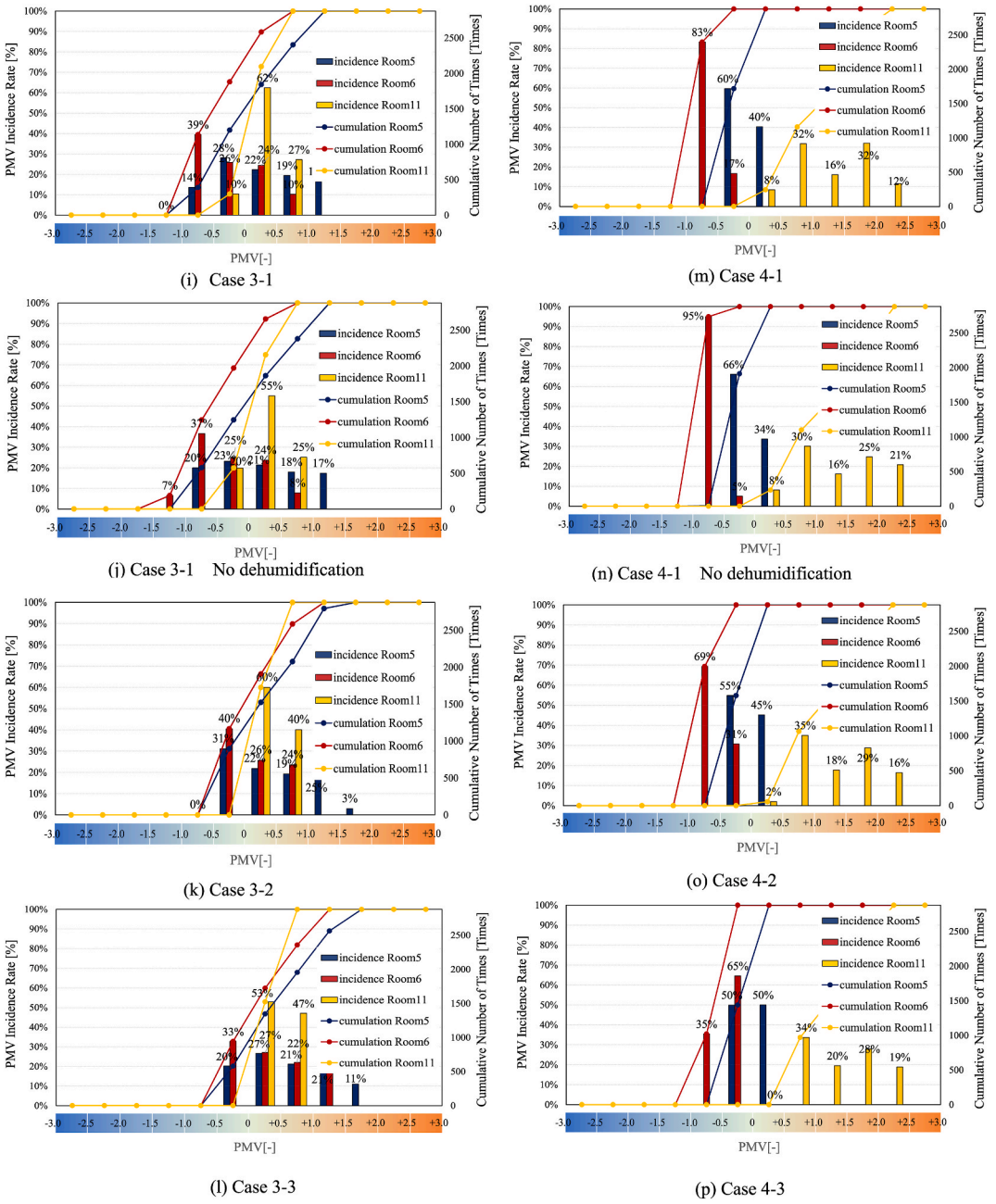

Fig. 14. (*continued*).

5.5.2. *Power consumption predictions and discussion results for air conditioners and radiant panels*

Fig. 15 shows a comparison of the integrated power consumption of the air conditioners for two days. This section compares the integrated power consumption of convection and radiant air conditioners for two days to identify the predominant difference between cases.

5.5.2.1. Comparison of representative Cases 1 to 4 (water supply temperature 7 °C). The overall trend in Cases 1-1 through 4-1 showed large power consumption levels for the radiant panels. The heat input into the space decreased with the number of panels. The COPs at the rating were 5.18 [-] for the air conditioners and 2.78 [−] for the radiant panels, which indicated the reason for the higher power consumption by the radiant panels. There was no difference in the heat input in the cases where the air conditioners on the second floor were operated. However, this was because the heat load calculated by THERB for the second floor was used as a reference. The heat quantity diffusion coefficient was concentrated on the second floor; therefore, the heat load on the second floor was considered in this

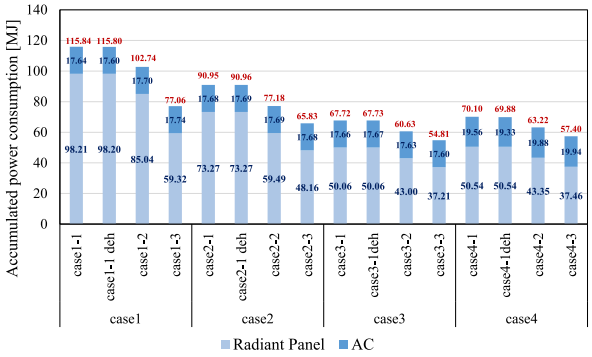

Fig. 15. Comparison of two-day total energy consumption of air conditioners.

case. Convergence calculations may be necessary depending on the actual operational conditions. For Case 4, the air conditioner and radiant panel were mixed on the first floor such that the air conditioner covered a certain load. In the calculation algorithm, the heat load of the air conditioner was calculated by considering the convection of the radiant panels and multiple reflections attributed to thermal diffusion and radiation (Gebhart's absorption coefficient). Therefore, in Case 4, the power consumption of the air conditioner increased by 2 MJ.

5.5.2.2. Sensitivity analysis of water supply temperature for radiant panels in Cases 1 to 4. A sensitivity analysis was performed when the water supply temperatures were changed to 11 °C and 15 °C. The power consumption of the radiant panels decreased when the temperature increased, and that of the air conditioner increased slightly. In Case 4, the power consumption of the air conditioner increased by approximately 2 MJ. Although the total power consumption trends of Cases 3 and 4 were similar, as shown in Fig. 15, it was necessary to consider the combination of comfort and power consumption.

5.5.2.3. Comparison of the impact of dehumidification in representative Cases 1 to 4 (water supply temperature 7 °C). The degree of influence on power consumption with and without dehumidification was evaluated in representative cases. As shown in Fig. 13(a), the air conditioner dehumidified only in Case 4. This indicated an increase in processed heat, which affected power consumption. However, the difference between power consumption with and without dehumidification was approximately 0.23 MJ, which was not considered large. The effect on the power consumption was negligible.

5.5.3. Optimal operation method for air conditioners and radiant panels

In Sections 4.5.1 and 4.5.2, comfort and energy efficiency were investigated using the thermal environment analysis method for the combined use of air conditioners and radiant panels. In this section, an optimal operation method that satisfies both comfort and energy efficiency and the case-by-case analysis are discussed.

5.5.3.1. Optimal operation method considering both comfort and energy efficiency. If only comfort was considered, Case 3-2 showed a relatively high median value, whereas Case 1–3 showed that for the second floor. This was because of the large area of the wall surface in contact with outside air, which varied from day to night. Case 1–3 showed a relatively low value of 77.06 MJ in the comparison of the integrated energy consumption, whereas Case 3-2 showed an even lower value of 60.43 MJ. In all cases, except for Case 4, the median value was higher when the water supply temperature was 11 °C. In Case 4, the difference in PMV in terms of the water supply temperature was insignificant; however, the median value was lower than that in Case 3-2, which was 15 °C. The median value was observed on the first floor when the water temperature was 15 °C. In contrast, Case 4-3 saved energy in terms of the integrated power consumption at 57.4 MJ. Considering the increase in the whole-building air conditioning, Case 3-2 satisfied both comfort and energy efficiency simultaneously, based on the results of the integrated power consumption. However, the energy efficiency was based on a relative comparison.

6. Conclusions

After investigating the effect of incorporating dehumidification, the proposed method was applied to a case study to determine the optimal operation method that satisfies both comfort and energy efficiency. The accuracy of the coupling method was improved by considering dehumidification, which was particularly important for achieving comfort. Additionally, we examined the contribution of dehumidification to comfort, noting that no significant difference was observed because of the high insulation performance of houses. However, the effect of this difference on insulation performance was beyond the scope of this study.

The importance of dehumidification varies depending on the required level of accuracy and could become more prominent if moisture-absorbing or dehumidifying materials were incorporated into the walls. Nevertheless, the results of this study do not undermine the need for dehumidification measures. The impact on power consumption was limited to Case 4, wherein the air conditioner provided dehumidification. This was because dehumidification led the air conditioner to bear the total heat load resulting from solar

radiation. The difference in the power consumption of the air conditioner with and without dehumidification was 0.23 MJ. It was assumed that the environmental impact on energy efficiency was not significant. However, under different conditions, such as when only the air conditioner is in operation, the effect on power consumption is expected to increase.

The use of three radiant panels resulted in overcooling in the occupied areas, specifically Rooms 5 and 6. However, the median PMV value was improved by increasing the water supply temperature. Case 1 exhibited higher power consumption than Cases 2–4. Although a relative comparison of integrated power consumption was provided, determining the significance of subtle differences was largely dependent on the energy field, which is beyond the scope of this study. Cases 3 and 4 showed relatively low integrated power consumption. However, in Case 4, the discomfort caused by the draft produced by the air conditioner could not be ignored and the comfort level on the second floor was inadequate, making this operating method unsuitable considering the proliferation of whole-building air conditioning in modern times. Therefore, Case 3 was deemed more appropriate in terms of energy efficiency and comfort. The comfort level remained within the 7-point rating owing to the highly insulated design of the house. While the case study holds some validity for the thermal environment analysis under the combination of radiant panels and air conditioning, which is in line with the current situation, a more detailed analysis is required to determine whether such a combination is ideal. Further investigation into the temperature of the supply water is recommended as well.

The proposed method offers a useful approach that can be applied when planning various housing types, ideally during the design stage. It can be particularly valuable for analyzing large spaces, such as libraries where a certain level of effective dehumidification is required.

Despite its potential applications, future works should address some issues with the proposed model. The model does not individually consider air conditioners or radiant panels, because the focus was on the operational scheme, excluding other operations. Future studies should compare scenarios involving various equipment and devices. A, it is necessary to explore how boundary conditions are established for air conditioners, using the equipment characteristics model developed by the Central Research Institute of the Electric Power Industry. Finally, the dehumidification algorithm should be made more relevant when applied to buildings that employ moisture-absorbing and desorbing materials.

Author contribution statement

Tatsuhiro Yamamoto, Dr: Conceived and designed the experiments; Performed the experiments; Analyzed and interpreted the data; Wrote the paper.

Akihito Ozaki: Conceived and designed the experiments; Contributed reagents, materials, analysis tools or data; Wrote the paper.

Keigo Aratsu: Performed the experiments; Analyzed and interpreted the data.

Ryo Fukui: Analyzed and interpreted the data; Wrote the paper.

Data availability statement

The authors do not have permission to share data.

Funding statement

This study was partially supported by Japan Society for the Promotion of Science (JSPS) KAKENHI [grant number JP19K23559].

Declaration of competing interest

The authors declare that they have no known competing financial interests or personal relationships that could have appeared to influence the work reported in this paper

Abbreviations

CFD	computational fluid dynamics
CL	ceiling
ES	energy simulation
FL	floor
HAM	heat–air–moisture
THERB	thermal environment of residential buildings

References

[1] United Nations, Sustainable development goals. https://www.un.org/sustainabledevelopment/sustainable-development-goals/, n.d (accessed 20 August 2021).

[2] U.S. Energy Information Administration, Residential energy consumption Survey (RECS). https://www.eia.gov/consumption/residential/ n.d. (accessed 20 August 2021).

[3] A. Majeed, L. Wang, X. Zhang, D. Muniba, D. Kirikkaleli, Modeling the dynamic links among natural resources, economic globalization, disaggregated energy consumption, and environmental quality: fresh evidence from GCC economies, Resour. Pol. 73 (2021), 102204, https://doi.org/10.1016/j.resourpol.2021.102204.
[4] Z. Huang, H. Zhang, H. Duan, How will globalization contribute to reduce energy consumption? Energy 213 (2020), 118825 https://doi.org/10.1016/j.energy.2020.118825.
[5] C. Chen, M. Pinar, T. Stengos, Determinants of renewable energy consumption: importance of democratic institutions, Renew. Energy 179 (2021) 75–83, https://doi.org/10.1016/j.renene.2021.07.030.
[6] O.A. Ismail, M.A. Kassem, M.A. Hassan, Sleeping pods with radiant cooling panels: a first assessment of thermal comfort and cooling capacity, Energy Build. 250 (2021), 111282, https://doi.org/10.1016/j.enbuild.2021.111282.
[7] M. Ye, A.A. Serageldin, A. Radwan, H. Sato, K. Nagano, Thermal performance of ceiling radiant cooling panel with a segmented and concave surface: laboratory analysis, Appl. Therm. Eng. 196 (2021), 117280, https://doi.org/10.1016/j.applthermaleng.2021.117280.
[8] T. Ueno, H. Kitahara, T. Miyanaga, Development of heat source characteristic model of air conditioner for residential buildings, in: Proceedings of ROOMVENT, São Paulo, Brazil, 2014.
[9] Q. Cheng, H. Feng, H. Meng, H. Zhou, CFD study of the effect of inlet position and flap on the airflow and temperature in a laying hen house in summer, Biosyst. Eng. 203 (2021) 109–123, https://doi.org/10.1016/j.biosystemseng.2021.01.009.
[10] C. Chen, C. Gorlé, Full-scale validation of CFD simulations of buoyancy-driven ventilation in a three-story office building, Build. Environ. 221 (2022), 109240, https://doi.org/10.1016/j.buildenv.2022.109240.
[11] M. Liu, R. Ooka, W. Choi, S. Ikeda, Experimental and numerical investigation of energy saving potential of centralized and decentralized pumping systems, Appl. Energy 251 (2019), 113359, https://doi.org/10.1016/j.apenergy.2019.113359.
[12] T. Djukic, M. Topalovic, N. Filipovic, Validation of lattice Boltzmann based software for blood flow simulations in complex patient-specific arteries against traditional CFD methods, Math. Models Comput. Simul. 203 (2023) 957–976, https://doi.org/10.1016/j.matcom.2022.07.027.
[13] T. Seshaiah, B. Vasu, K.V.K. Kumar Reddy, P. Bridjesh, Analysis on air craft winglet at different angles by using CFD simulation, Mater. Today 49 (2022) 275–283, https://doi.org/10.1016/j.matpr.2021.02.073.
[14] L. Tool. https://www.mlit.go.jp/gobuild/sesaku_lcem_lcemtool_index.htm.
[15] M.C. Katafygiotou, D.K. Serghides, Analysis of structural elements and energy consumption of school building stock in Cyprus: energy simulations and upgrade scenarios of a typical school, Energy Build. 72 (2014) 8–16, https://doi.org/10.1016/j.enbuild.2013.12.024.
[16] Y. Hu, Y. Peng, Z. Gao, F. Xu, Application of CFD plug-ins integrated into urban and building design platforms for performance simulations: a literature review, Front. Archit. Res. (2022), https://doi.org/10.1016/j.foar.2022.06.005.
[17] Z. Jing, L. Jiayu, Study on heat transfer delay of exposed capillary ceiling radiant panels (E-CCRP) system based on CFD method, Energy Build. 180 (2020), 106982, https://doi.org/10.1016/j.buildenv.2020.106982.
[18] Z. Zhai, Q. Chen, P. Haves, J.H. Klems, On approaches to couple energy simulation and computational fluid dynamics programs, Build. Environ. 37 (2002) 857–864, https://doi.org/10.1016/s0360-1323(02)00054-9.
[19] Z.J. Zhai, Q.Y. Chen, Performance of coupled building energy and CFD simulations, Energy Build. 37 (2005) 333–344, https://doi.org/10.1016/j.enbuild.2004.07.001.
[20] T. Yamamoto, A. Ozaki, M. Lee, K. Aratsu, R. Fukui, Development of a non-stationary thermal environment analysis method for combined convection and radiation air conditioning, Build. Environ. 207 (2022), 108559, https://doi.org/10.1016/j.buildenv.2021.108559.
[21] T. Yamamoto, A. Ozaki, M. Lee, Optimal air conditioner placement using a simple thermal environment analysis method for continuous large spaces with predominant advection, Energies 14 (2021) 4663, https://doi.org/10.3390/en14154663.
[22] Y. Fan, K. Ito, Energy consumption analysis intended for real office space with energy recovery ventilator by integrating BES and CFD approaches, Build. Environ. 52 (2012) 57–67, https://doi.org/10.1016/j.buildenv.2011.12.008.
[23] T. Yamamoto, A. Ozaki, K. Aratsu, Advanced thermal environment and energy consumption calculation over time using combined energy simulation, computational fluid dynamics, and heat source model, J. Build. Perform. Simul. 14 (2021) 619–645, https://doi.org/10.1080/19401493.2021.1992503.
[24] T. Yamamoto, A. Ozaki, M. Lee, Development of a thermal environment analysis method for a dwelling containing a colonnade space through coupled energy simulation and computational fluid dynamics, Energies 12 (2019) 2560, https://doi.org/10.3390/en12132560.
[25] S. Kato, S. Murakami, H. Kobayashi, New scales assessing contribution of heat sources and sinks to temperature distributions in room by means of numerical simulation, in: Proc. 4th Int. Conf. On Air Distribut. in Rooms (ROOMVENT94), Kraków, Poland, 1994, pp. 1–19.
[26] A. Ozaki, T. Watanabe, T. Hayashi, Y. Ryu, Systematic analysis on combined heat and water transfer through porous materials based on thermodynamic energy, Energy Build. 33 (2001) 341–350, https://doi.org/10.1016/S0378-7788(00)00116-X.
[27] B. Gebhart, A new method for calculating radiant exchanges, Build. Eng. 165 (1959) 321–332.
[28] International Organization for Standardization, ISO 7730:2005 Ergonomics of the thermal environment - analytical determination and interpretation of thermal comfort using calculation of the PMV and PPD indices and local thermal comfort criteria Standardization. https://www.iso.org/standard/39155.html.